JOURNAL OF Materials CHEMISTRY

Chemical hydrogen insertion into CMD exhibiting low microtwinning

Lachlan A. H. MacLean† and Frank L. Tye*

Energy Technology Centre, Middlesex University, Bounds Green Road, London UK N11 2NQ. E-mail: F.Tye@mdx.ac.uk

Received 4th August 2000, Accepted 12th December 2000
First published as an Advance Article on the web 12th February 2001

Hydrogen has been inserted into a γ-MnO_2 (CMD type) characterised by approximately 70% de Wolff disorder and a low amount of microtwinning. 22 compounds were prepared covering the range $0<s<0.88$ where s is the value in $MnO_{1.944}H_s$. XRD and FTIR studies showed homogeneous insertion up to $s=0.56$ and heterogeneous insertion above this level. The results have been compared with those published in a companion paper where the host γ-MnO_2 had 40% de Wolff disorder. For both materials, the onset of heterogeneous insertion occurred when the *a* lattice dimension, derived from the ramsdellite portions of the intergrowths, had increased, in the homogeneous region, to its value in the final product. An important finding was the evidence that insertion took place uniformly in both portions of the intergrowths and not preferentially into the ramsdellite parts. Another important finding was the sudden location of all inserted H to form OH bonds in the middle of the homogeneous insertion region. This contrasted with the absence of OH bond formation for $s<0.36$ and thereby strengthens the hypothesis of independent mobility of protons and electrons in regions where OH bond formation was absent. The concept of hinging again proved useful in interpreting the data and allowed the calculation of lattice parameters of the pyrolusite/manganite portions of the intergrowth from XRD data interpreted in terms of the ramsdellite/groutite portions of the intergrowth. Hinging is here defined as the equal clockwise and anti-clockwise rotation of two edge-shared octahedral chains about the *c*-directed axis connecting them.

Introduction

Glemser[1] was the first to identify a form of manganese dioxide that differed in X-ray diffraction (XRD) pattern from pyrolusite and ramsdellite which he called γ-MnO_2. Today, two different types of γ-MnO_2's are manufactured commercially for use in batteries: one is produced by electrodeposition[2] (EMD) and the other by a chemical route[3] (CMD). Byström[4] suggested that γ-MnO_2 was an 'intermediate product between pyrolusite and ramsdellite'. The accuracy of this suggestion was strikingly confirmed for ramsdellite rich intergrowths by de Wolff[5] who linked the broadening and peak shift of certain XRD lines (those with *k* odd in the *hkl* nomenclature) in the ramsdellite pattern with the proportion of pyrolusite in the intergrowth structure. The samples of γ-MnO_2 that were used in de Wolff's study had line rich XRD patterns and are not readily connected with EMD which has only five main and one minor XRD lines.[6] This difficulty was eventually resolved by Pannetier *et al.*[7–10] who concluded that extensive microtwinning of the intergrowth structure across the 021 and/or 061 planes leads to peak overlap and simplification of the XRD pattern towards that observed with EMD.

An unfortunate consequence of the present position is that very little direct information on the unit cell structures of either the ramsdellite or the pyrolusite portions of the intergrowth can be obtained from the XRD patterns of γ-MnO_2's that are heavily microtwinned, such as EMD, as all the XRD lines other than 200 are shifted.[10] This, however, is not the case for γ-MnO_2's that have much less microtwinning. For these, the so-called 'sharp' lines, *i.e.* those with $(0.5k+l)$ even are not shifted and may be used to derive the unit cell dimensions of the ramsdellite part of the intergrowth structure. A study of one such material, coded SBPA and made electrochemically by a suspension bath process,[11] has already been reported.[12] The purpose of this work is to report on another, Faradiser M, made commercially[3] and which differs from SBPA in having a higher proportion of pyrolusite in the intergrowth.

Interpretation of H insertion in the earlier paper[12] was considerably aided by the introduction of a grid which directly linked unit cell dimensions *a* and *b* of the ramsdellite part of the intergrowth to the apical expansion of ramsdellite octahedra in the direction normal to the *c* axis and to the angle β this apical line made with the *b* direction at the corner connections of the double octahedral chains. The apical line and the angle β are defined by Fig. 1. The term hinging was used to describe changes in angle β.[12] In the previous work,[12] a large hinging rotation in the heterogeneous region at high H insertion levels was associated with OH bond formation (identified by FTIR). The consequent change in tunnel shape suggests that hydrogen bonding with oxygens at O(1) positions occurred as well as a coordinate bonding with oxygens at O(2) positions as originally envisaged almost 20 years ago.[13]

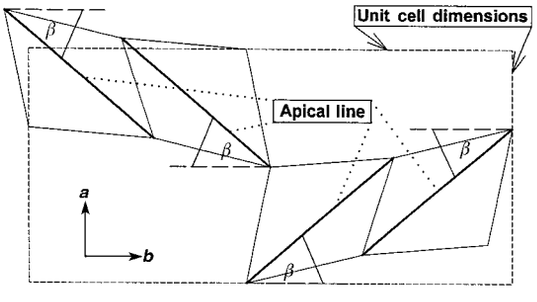

Fig. 1 Identification of apical line and angle β for the ramsdellite/groutite part of the intergrowth.

†Present address: Cedalion Ltd., 27 Maritime Street, Edinburgh, UK EH6 6SE.

DOI: 10.1039/b006408o

Table 1 Characteristics of Faradiser M

Characteristic	Value	Reference
n in MnO_n	1.944	This work
% Microtwinning	~10	10 (Tables 2–4)
% de Wolff disorder	~70	10 (Tables 2–4)
BET specific surface area/$m^2\ g^{-1}$	93	14

Experimental

Material

The commercial CMD used as the starting material in this study was Faradiser M supplied by SEDEMA of Belgium. Some characteristics of this material are given in Table 1.

H-Insertion

The level of H-insertion into a manganese dioxide of initial oxidation state MnO_n is described by the symbol s in reaction (1).

$$MnO_n + sH^+ + se^- \rightarrow MnO_nH_s \quad (1)$$

For the reasons given previously[15] this convention is now preferred[12,15] to an earlier one[16–18] based on reaction (2),

$$MnO_2 + rH^+ + re^- \rightarrow MnOOH_r \quad (2)$$

which presumes that the initial oxidation state is less than two due to some initial H-insertion.

Chemical H-insertion was carried out by the methods described in the companion paper.[12] The reagents and conditions used are outlined in Table 2. The higher levels of insertion up to the theoretical maximum of $s=0.89$ were obtained by refluxing in propan-1-ol. Under these conditions, H-insertion occurred approximately twice as fast in Faradiser M as in SBPA[12] and a full range of 22 insertion levels was achieved without recourse to reflux in the higher boiling butan-1-ol (bp 118 °C) as had been required with SBPA. The higher BET surface area of Faradiser M, 93 as compared with 22 $m^2\ g^{-1}$ for SBPA, is likely to have been one of the factors responsible for this difference; another is presented later in this paper.

Characterisation

The H-inserted samples were analysed for oxidation state and their X-ray diffraction patterns (Philips PW 1700 powder X-ray diffractometer) and their FTIR spectra (Perkin Elmer PE 1750 FTIR spectrometer) were determined. The procedures used were precisely those described in the earlier publication.[12] The level of H-insertion, s, was calculated from the oxidation states, before (MnO_n) and after (MnO_x) H-insertion, using the relationship in eqn. (3)

$$s = 2(n-x) \quad (3)$$

Table 2 Conditions and reagents used for H-insertion

Reagent	Temperature/°C	Time	s
Acetone	20	0 to 30 s	0–0.24
Propan-1-ol	20	2 to 3.5 min	0.37–0.40
Propan-1-ol	43	2 to 8 days	0.44–0.74
Propan-1-ol	97	0.5 to 10 h	0.35–0.88

Results and discussion

Evidence for regions of homogeneous and heterogeneous H-insertion

Although the XRD patterns of the H-inserted materials were obtained in the range $15° < 2\theta(\text{Cu-K}\alpha) < 80°$, identification of the insertion level at which a change in the pattern took place is better seen by viewing the 2θ range 33 to 44° shown in Fig. 2. The patterns are stepped down the figure by an amount proportional to the level of H-insertion. The patterns are almost identical apart from a slight shift of peaks to lower values of 2θ up to insertion levels of $s=0.54$. At higher insertion levels the XRD pattern changes shape and new peaks emerge.

Fig. 3(A) shows the extent of peak shift in the lower H-insertion region where the patterns keep essentially the same shape. This behaviour is consistent with homogeneous H-insertion such that a single phase is maintained and the crystalline structure is little changed apart from the dilation indicated by the peak shift. Brenet *et al.*[19] were the first to observe and interpret this behaviour for γ-MnO_2 and it has since been reported a number of times.[12,18–22]

Fig. 3(B) compares XRD patterns at the beginning and end of the region in which H-insertion caused the shape of the pattern to change. This is the region of heterogeneous H-insertion. Some values of 2θ where the patterns cross are noted in the figure: these are isosbestic points. In this region, the same two phases were present at all times and insertion of H converted a proportion of the lower H-inserted phase ($s \approx 0.59$) into the higher H-inserted phase ($s \approx 0.88$). The constant intensity at the isosbestic points in the heterogeneous H-insertion region is shown in Fig. 4. This constancy confirms the presence of a mixture of the two end-members throughout this region.

The boundary between homogeneous and heterogeneous

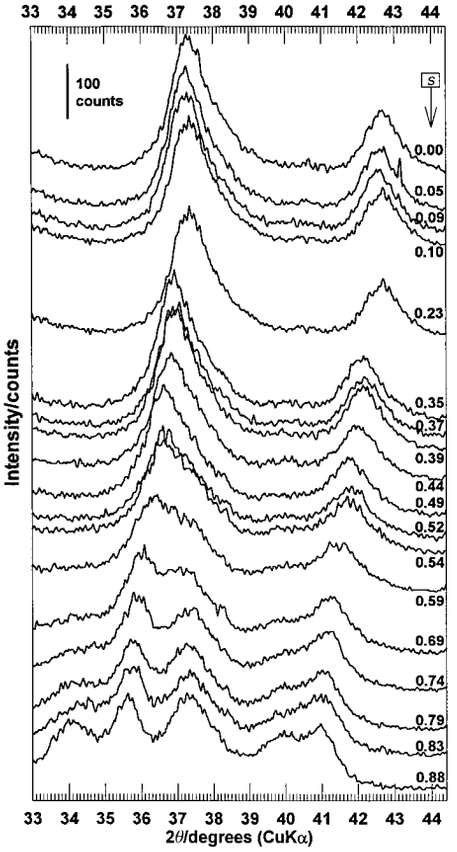

Fig. 2 XRD patterns of H-inserted Faradiser M in the region $33° < 2\theta < 44°$ stepped in proportion to the insertion level.

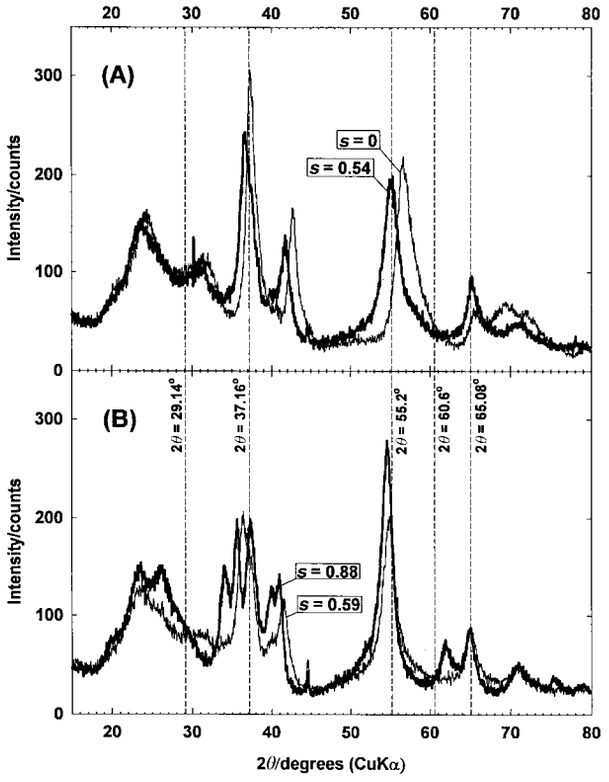

Fig. 3 Comparison of XRD patterns at the extremes of the regions of (A) homogeneous and (B) heterogeneous H-insertion. Dashed lines denote 2θ values which are isosbestic in the heterogeneous region.

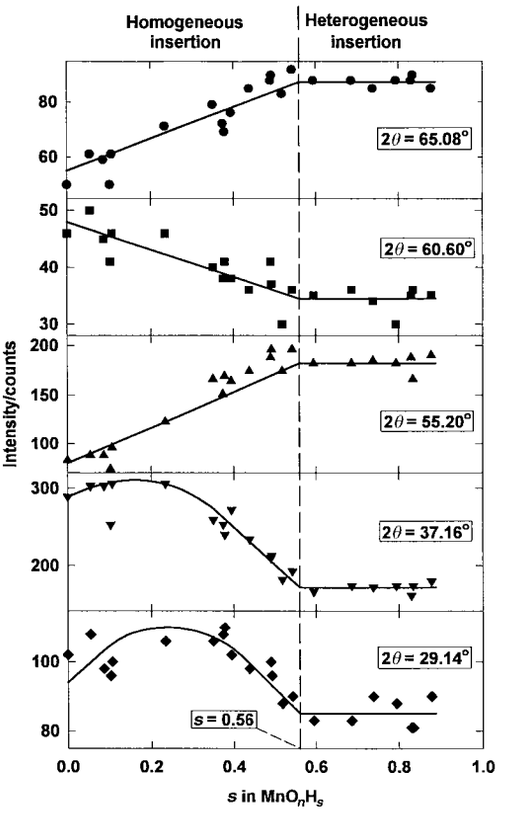

Fig. 4 Intensity *versus* H-insertion at 2θ values which are isosbestic in the region of heterogeneous insertion.

insertion is shown as $s=0.56$ in Fig. 4. The intensity at the isosbestic points varies in the homogeneous region in a way that depends on the position of the isosbestic value of 2θ relative to an XRD peak at the beginning of the homogeneous region. This is made clearer by reference to Fig. 3, which marks the values of 2θ that were isosbestic in the heterogeneous region and reveals their behaviour in the homogeneous region of peak movement. Thus $2\theta=65.08^\circ$ is situated on the low angle side of a peak in the starting material and as the peak shifts to lower angles with homogeneous H-insertion, intensity increased as noted in Fig. 4. An identical argument explains the movement in the homogeneous region for $2\theta=55.2^\circ$. On the other hand, if the value of the isosbestic 2θ is situated on the high angle side of a peak in the starting material then its intensity falls during homogeneous H-insertion. An isosbestic 2θ of this type is found at 60.6°. When an isosbestic 2θ is situated on the low angle side of the XRD peak at the commencement of homogeneous H-insertion and on the high angle side of the peak at the completion of homogeneous H-insertion then its intensity increases initially and then falls. This is observed at $2\theta=37.16^\circ$.

An alternative method of identifying the boundary between homogeneous and heterogeneous H-insertion is to plot the intensity of the new XRD peaks that emerge in the heterogeneous region. This plot, presented as Fig. 5, confirms that the boundary is at about $s=0.56$. In an attempt to minimise statistical counting errors, the average counts at 10 values of 2θ on either side and including the peak were used for this plot.

FTIR spectra are conveniently divided into two regions by the wavenumber $800\,\mathrm{cm}^{-1}$. Below $800\,\mathrm{cm}^{-1}$, the FTIR absorption bands of these structures are a consequence of octahedral vibrations, and above are due to OH bond vibrations.[15,23] H-Insertion caused few changes to the positions and shape of absorption bands due to octahedral vibrations in the homogeneous region. However, changes in the heterogeneous region of H-insertion permitted the identification of isosbestic points. This is shown in Fig. 6 and plots of the absorbance values at the wavenumbers of the isosbestic points, 544, 588 and $652\,\mathrm{cm}^{-1}$, are shown in Fig. 7. These plots support the conclusions already reached on the basis of XRD that the boundary between homogeneous and heterogeneous H-insertion is at about $s=0.56$.

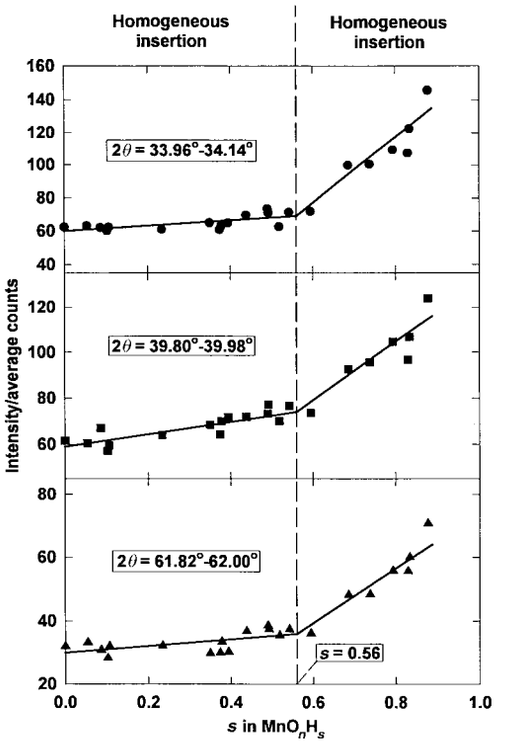

Fig. 5 Growth of new XRD peaks in the region of heterogeneous H-insertion.

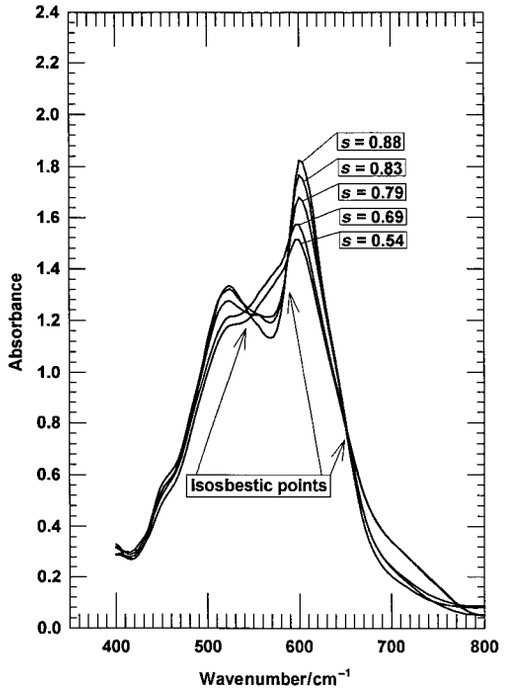

Fig. 6 isosbestic points in the FTIR spectra from octahedral vibrations in the heterogeneous region of H-insertion.

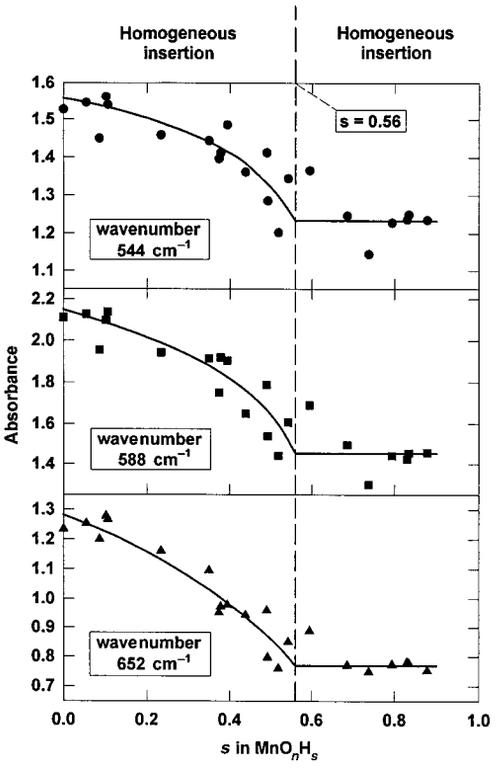

Fig. 7 Absorbance *versus* H-insertion level at three wavenumbers that are isosbestic above $s=0.56$.

OH bond formation

Fig. 8 compares the FTIR spectra above 800 cm^{-1} of the most H-inserted sample of Faradiser M with manganite (γ-MnOOH),[24] groutite (α-MnOOH)[24] and the most H-inserted sample of SBPA.[12] Examination of the wavenumber region 900 to 1200 cm^{-1} is particularly illuminating. Manganite has OH bending vibrations[23] at 1088 and 1152 cm^{-1} that are shifted in groutite[23] to 998 and 1030 cm^{-1}. The shift is presumably due to the different local environments presented by the 2×1 tunnels of groutite/ramsdellite as compared with the 1×1 tunnels of manganite/pyrolusite. Fully H-inserted products of γ-MnO_2, known as δ-MnOOH,[13] are intergrowths of manganite and groutite having both 1×1 and 2×1 tunnels, and would therefore be expected to have both sets of vibrations. Thus Faradiser M, H-inserted to $s=0.88$, has the manganite bands at 1088 and 1152 cm^{-1} and a prominent shoulder in the position of the groutite bands. With SBPA, H-inserted to $s=0.81$, the situation is reversed with the groutite bands having greater prominence than the manganite bands. Clearly, Faradiser M has a greater proportion of pyrolusite in its intergrowth structure than does SBPA. As shown in Fig. 8, other bands that are unique to either manganite or groutite lead to the same conclusion. It is worth remarking that direct evidence of the intergrowth structure of γ-MnO_2, as is here revealed by FTIR, is scarce. The peak values noted in Fig. 8 for manganite and groutite are very close to those recently reported for mineralogical specimens.[23]

Fig. 9 shows FTIR spectra above 800 cm^{-1} for Faradiser M inserted with varying levels of H. The most interesting observation is that the spectra do not take on the character of fully H-inserted material until the level of insertion is $s=0.37$. In particular, the OH bending band[23] at 2035 cm^{-1} and the OH stretching band[23] at 2690 cm^{-1} are absent at all levels of insertion up to and including $s=0.35$. In fact, the insertion of H had little effect on the spectra up to and including $s=0.35$ apart from an increase in the peak at 1415 cm^{-1}, which, along with the peak at 1548 cm^{-1}, probably did not arise from OH vibrations and are thought to be overtones of octahedral vibrations.[15] The fact that the absorbances of the 1415 and 1548 cm^{-1} bands changed little, if at all, between $s=0.23$ and full insertion at $s=0.88$, supports this suggestion. The conclusion already reached in studies on other γ-MnO_2/δ-MnOOH systems,[12,15] is that at the lower levels of H-insertion, OH bond formation does not take place and mobile protons are present in the homogeneous phase.

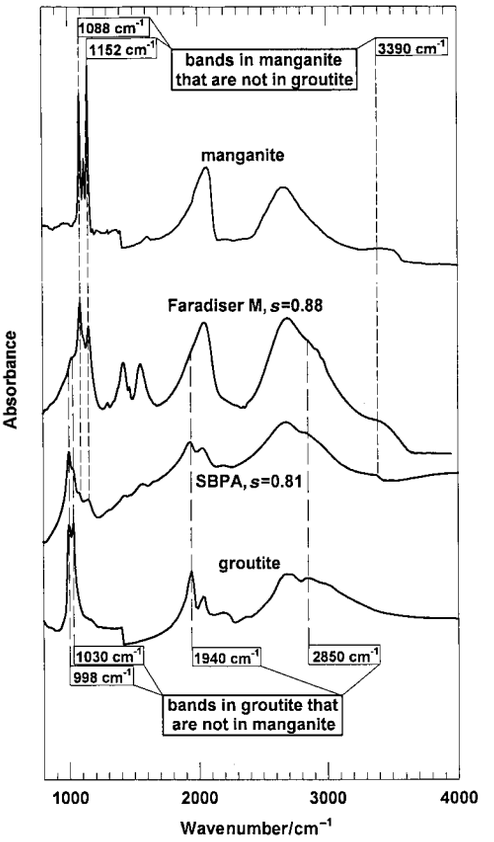

Fig. 8 Comparison of FTIR OH vibrations of fully H-inserted Faradiser M and SBPA[12] with manganite[24] and groutite.[24]

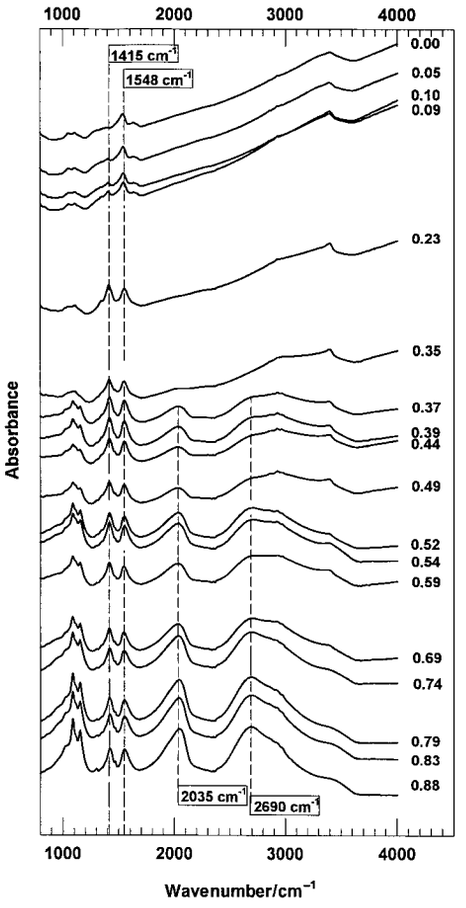

Fig. 9 FTIR OH vibrations of H-inserted Faradiser M stepped in proportion to the insertion level.

As in previous publications,[12,15] the progress of OH bonding was examined by plotting the area under peaks in three regions: here 875–1250, 1740–2270 and 2268–3348 cm^{-1}. The background, as estimated from a line joining the boundaries of the region, was subtracted from the total area to give the area under peaks. The plots are shown in Fig. 10. The important new observation is the jump in peak area between $s=0.35$ and $s=0.37$, which is drawn in the figure as a jump at $s=0.36$. Below $s=0.36$ there are no OH bonding peaks as is evident from Fig. 9: the small areas noted in Fig. 10 are due only to slight curvature of the FTIR spectral line. At $s=0.36$ the environment in the tunnels had changed sufficiently to allow *all* of the previously inserted H to locate and OH bonds were formed; hence the jump. Interestingly, the location of inserted H at $s=0.36$ occurred in the middle of the homogeneous H-insertion range which extended to $s=0.56$. Thus, in the region of homogeneous insertion, H was initially present as a mobile constituent but did not form OH bonds and then, as more H was inserted, all of the H located. The phase however remained homogeneous so the located H must have remained mobile, hopping from one OH bond to the next. It is tempting to relate these two situations to the number of thermodynamically independent components arising from the insertion of H. For $s<0.36$, the inserted H was present as protons and electrons that were independently mobile, a hypothesis which has been successful[25–27] in explaining the large extent of the decrease in electrode potential of EMD on discharge. For $0.36<s<0.56$, the inserted H was a present as a single component with protons and electrons diffusing together to adjacent Mn^{4+} and O^{2-} sites. Such an assumption was used to explain the 50% fall in potential of β-MnO_2 as compared with EMD with small amounts of inserted H.[28]

The jump which occurred at $s=0.36$ in Fig. 10 and signalled

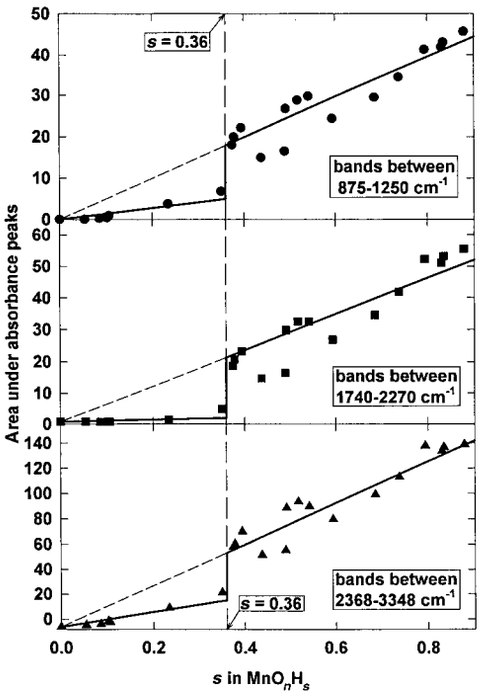

Fig. 10 Integrated net peak areas of FTIR spectra *versus* H-insertion level.

H location in Faradiser M was not present in similar studies on EMD[15] or SBPA.[12] The reason is that in the earlier studies H location was only present in the final product and OH bonding absorptions therefore grew only in the heterogeneous region from essentially zero as the proportion of the final fully inserted product grew with insertion in the two-phase system. It follows that this work is the first which has allowed examination of OH bonding vibrations at different H-insertion levels in order to ascertain whether 1×1 or 2×1 tunnels offer preferred sites for H location. Fig. 11 compares the FTIR spectra of H-insertion compounds at $s=0.38$ when H had just located; at the end of homogeneous insertion, $s=0.54$, and the final product at the end of heterogeneous insertion, $s=0.88$. The comparison is made for the critical region 950–1200 cm^{-1} which contains both manganite and groutite vibrations. Absorbances are adjusted by a factor to aid comparison and to allow for the different amounts of H located in the compounds. The first thing to note from Fig. 11 is that from the point at which H initially located, $s=0.38$, both manganite and groutite vibrations were present. Clearly H located in both 1×1 and 2×1

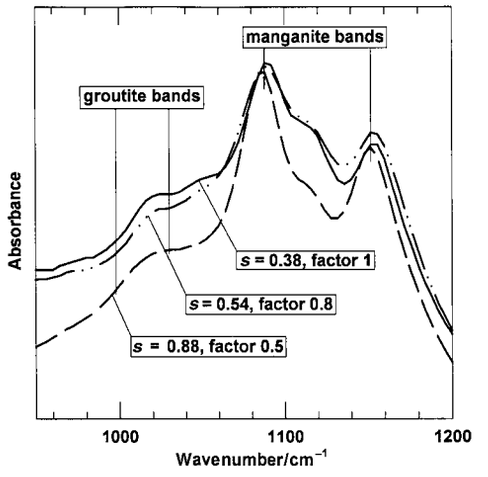

Fig. 11 Comparison of shapes of FTIR OH spectra for Faradiser M at some critical H-insertion levels.

tunnels. Furthermore near the end of the homogeneous region of H-insertion, at $s=0.54$, the shape of the FTIR spectra was virtually indistinguishable from that at $s=0.38$. The conclusion to be drawn is that as soon as the structural conditions were suitable for location, all of the inserted H partitioned itself between the 1×1 and 2×1 tunnels and then maintained the same degree of partitioning throughout the region of homogeneous insertion. The same degree of partitioning was probably present in the fully inserted product, $s=0.88$, but the sharpening of the manganite peaks makes the comparison more difficult. The important overall conclusion is that for this intergrowth structure the evidence is against preferential H entry and location in 2×1 tunnels. Preferential discharge of the ramsdellite portion of an intergrowth is a key postulate in the theories promulgated by Chabre and Pannetier.[8,10]

Structural aspects

Five peaks were available in the homogeneous region of H-insertion for calculating unit cell parameters: those at 2θ values of about 37, 43, 57, 65 and 69° [see Fig. 3(A)]. These peaks were asymmetric indicating the presence of hidden peaks. The peak positions were therefore refined using the deconvolution program Win Fit! (© S. Kramm) and a Pearson VII profile. These lines may be assigned either to the ramsdellite/groutite or to the pyrolusite/manganite part of the intergrowth. The estimate of 70% de Wolff disorder is not a convincing argument for adopting a pyrolusite/manganite lattice since each de Wolff or pyrolusite layer only contains half the number of manganese and oxygens that are contained in the equivalent ramsdellite/groutite layer. A more fundamental difficulty, however, is that none of the ground-breaking ideas of γ-MnO_2 intergrowth structures published by de Wolff and Laudy[5,29] and Pannetier *et al.*[7–10] have taken into account the hinging that must take place in the ramsdellite and/or pyrolusite portions of the structure to bring them to a common value for the *a* lattice parameter. For pyrolusite this means that the unit cell may change from tetragonal to orthorhombic symmetry (see Fig. 12). Reports of orthorhombic pyrolusite have appeared in the literature[5,24,30,31] and interestingly this form is usually associated with remnants of another structure able to cause hinging. Thus if pyrolusite/manganite were chosen as the structure to which the peaks should be assigned, each refined peak might need further deconvolution into two peaks to identify the *a* and *b* parameters of an orthorhombic unit cell. This is not realizable at the present time, given the nature of the XRD data available.

The above problem does not arise if ramsdellite/groutite is chosen as the structure responsible for the XRD lines as hinging alters the positions of the lines to reflect changed orthorhombic unit cell parameters but does not broaden or increase the number of lines. Computer simulations of intergrowth structures give more positive encouragement to the necessity of assigning the observed XRD lines to a ramsdellite/groutite structure. Two different simulations[10,32] have shown that the main pyrolusite line at $2\theta=28.7°$ does not appear until the pyrolusite fraction reaches 90% and also that the characteristic ramsdellite line at $2\theta=22.2°$ although shifted is retained until the pyrolusite fraction is 70%.

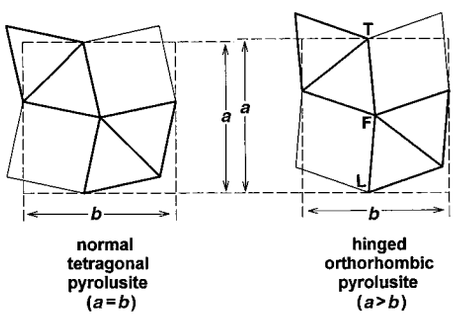

Fig. 12 Comparison of normal tetragonal pyrolusite with a hinged orthorhombic form.

The refined peaks at 2θ values of about 37, 43, 57, 65 and 69° were therefore assigned respectively to the 021, 121, 221, 002 and 061 planes of ramsdellite and the *a* and *b* unit cell parameters derived from them are plotted in Fig. 13 along with the grid showing expansion of the apical line and angle β (see Fig. 1), which was developed in a previous publication.[12] Also shown for comparison are the data published previously for the sample coded SBPA[12] plus the parameters for ramsdellite[33] and groutite.[34] The *c* parameters of the unit cells of all of the materials shown in Fig. 13 are virtually constant and predominantly fall in the range 2.85–2.87 Å, so all changes resulting from H-insertion or a different material can be fairly represented by considering only the *a* and *b* unit cell parameters. As noted previously with SBPA, there is some shortening of the *b* parameter also with Faradiser M, as is evident from the points falling below the zero expansion curve on which ramsdellite is situated. This was proved for SBPA to be due to the necessity of using only a restricted number of lines for calculating the unit cell parameters[12] and the same explanation probably applies to the data for Faradiser M.

A number of significant findings are revealed by careful consideration of Fig. 13. Because pyrolusite has an *a* dimension of 4.398 Å compared with 4.533 Å for the same parameter in ramsdellite, one or both parts of the intergrowth must hinge in order to reach a common value for *a*. In the case of SBPA, hinging reduced the *a* parameter of the ramsdellite portion from 4.533 to 4.446 Å. With Faradiser M, which has a greater fraction of pyrolusite in the intergrowth (see Table 1), ramsdellite hinging was even greater and the *a* parameter was reduced to a value which was close to the value for tetragonal pyrolusite. In view of this finding, an attempt was made to assign the refined peaks at 2θ values of about 37, 43,

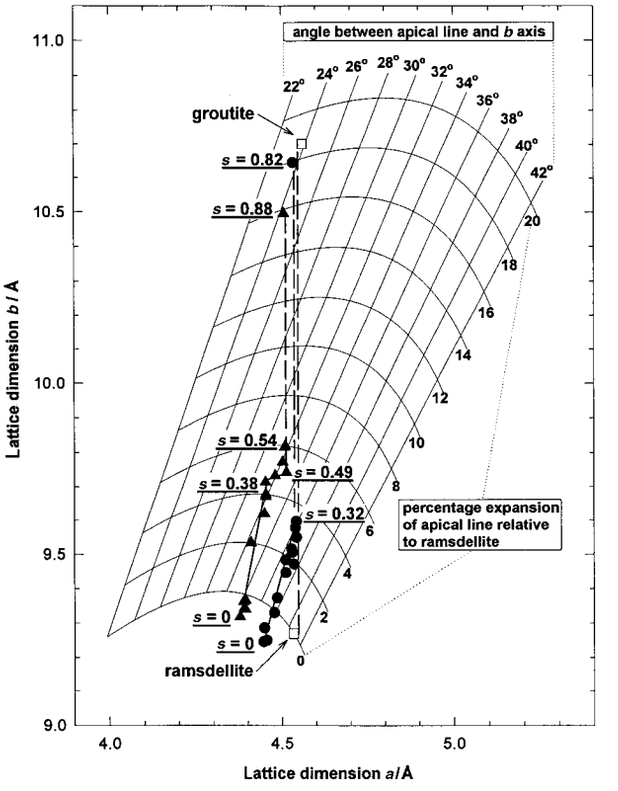

Fig. 13 Effect of H-insertion on expansion of the apical line and rotation of angle β of ramsdellite part of the intergrowth. ▲ Faradiser M, ● SBPA, ——— homogeneous insertion, — — — heterogeneous insertion.

57, 65 and 69° to the 101, 111, 211, 002 and 310 planes of a tetragonal pyrolusite unit cell but this yielded no coherent explanation of the data.

Returning to SBPA for a moment, it is clear from Fig. 12 that there is a limit to the extent to which hinging can increase the *a* parameter of pyrolusite. That limit is reached when the points T, F and L fall on the same *ac* plane: in other words, they form a straight line in the *a* direction on an *ab* projection. The maximum value of *a* for a hinged pyrolusite is twice TF and is 4.497 Å. H-insertion initially occurred homogeneously with SBPA and *a* increased steadily (see Fig. 13) with insertion level and reached the maximum possible *a* dimension for hinged pyrolusite at an insertion level between $s=0.17$ and $s=0.21$. Further insertion up to $s=0.34$ resulted in an increase in *a* to a value of 4.54 Å which is significantly above the maximum. This could only have arisen because insertion was taking place in both the pyrolusite and ramsdellite portions of the intergrowth and changing the dimensions of all octahedra by apical expansion. This evidence with SBPA thus complements the conclusions reached earlier in this paper for Faradiser M on the basis of OH bond vibrations that H-insertion occurred simultaneously in both parts of the intergrowth.

Further evidence that H was inserted into the pyrolusite and ramsdellite parts of the intergrowth in the homogeneous region without preference or selectivity for one structural type is provided by Fig. 14. Fig. 14 shows that the apical expansion of the octahedra of ramsdellite with H-insertion follows the same linear trend for both Faradiser M and SBPA. As Faradiser M has a substantially lower proportion of ramsdellite in the intergrowth than has SBPA this could only happen if H were inserted without preference throughout the octahedral content of the intergrowth, irrespective of whether octahedra were part of the single chains of pyrolusite or the double chains of ramsdellite.

The hinging of about 2° which occurred with Faradiser M between $s=0.38$ and $s=0.49$ (see Fig. 13) may have been a consequence of the H-insertion method. When insertion levels were approaching those required for the heterogeneous region, it is possible that some final product was produced in the regions adjacent to the hydrogen donor under the non-equilibrium conditions pertaining during insertion. Remnants of final product, albeit in insufficient amounts to give rise to XRD or FTIR peaks, could have caused hinging to bring the *a* lattice of the homogeneous phase towards that of the final product.

As was the case with SBPA, H-insertion became heterogeneous with Faradiser M when the *a* parameter had expanded by homogeneous insertion to the point at which its value became equal to the *a* parameter of the product. This coincidence, now with two quite different γ-MnO_2 intergrowths, reinforces the suggestion,[12] that heterogeneous insertion occurred by progression of the boundary between the two phases in the *b* direction across the *ac* planes. The inserted species were presumably transported at right angles along the *c* direction to the sites of conversion to the product: protons along the tunnels and electrons through the edge-shared octahedra.

The final part of the paper is a calculation of the *b* lattice parameters of the pyrolusite/manganite portion of the inserted intergrowth materials. The following steps and assumptions were required. H-Insertion occurred without preference into the tunnels and octahedra of the two parts of the intergrowth so that the overall level of insertion *s* applied also to each part of the intergrowth. The known octahedra, projected on the *ab* plane, of pyrolusite ($\mathbf{FD_pC_pH_p}$) and manganite ($\mathbf{FD_mC_mH_m}$) were placed so that apex **F** coincided and the apical lines $\mathbf{FC_p}$ and $\mathbf{FC_m}$ formed the same angle with the *b* axis as shown in Fig. 15(A). Inserted octahedra were then calculated using the following equalities [eqn. (4)] for the length ratios.

$$\mathbf{D_pD_s/D_pD_m = C_pC_s/C_pC_m = H_pH_s/H_pH_m = C_rC_s/C_rC_g}$$

$\mathbf{C_rC_g}$ is the increase in the apical distance of groutite minus that of ramsdellite and $\mathbf{C_rC_s}$ is the increase in apical length of the ramsdellite part of the intergrowth on H-insertion. Both of these lengths were available from Fig. 13 when combined with the information that the apical length of ramsdellite is 3.773 Å. Calculated inserted octahedra ($\mathbf{FD_sC_sH_s}$) were then rotated about **F** to position ($\mathbf{F\,{}^rD_s\,{}^rC_s\,{}^rH_s}$) as shown in Fig. 15(B). The length $\mathbf{{}^rH_sX}$ is exactly 50% of the unit cell dimension *a* and the amount of rotation was chosen so that the *a* dimension of the pyrolusite part of the intergrowth was identical with the *a*

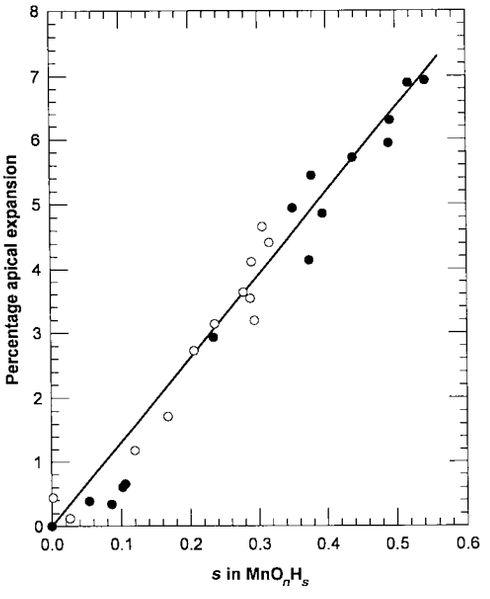

Fig. 14 Comparison of apical extension for Faradiser M and SBPA (ref. 12) in the homogeneous H-insertion region for the ramsdellite/groutite part of the intergrowth. ● Faradiser M, ○ SBPA.

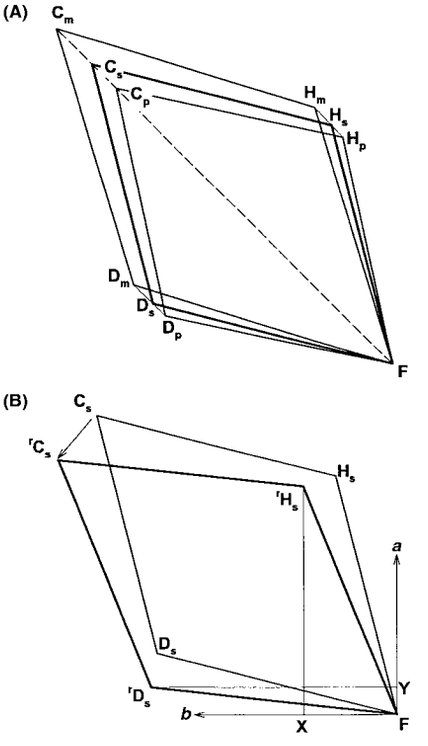

Fig. 15 Calculation of lattice dimension *b* of the pyrolusite part of the intergrowth. (A) Calculation of inserted octahedra, projected on *ab* plane. (B) Rotation of inserted octahedra.

dimension of the ramsdellite part of the intergrowth, deduced from the XRD data (see Fig. 13). The b dimension of the pyrolusite part of the intergrowth was then available as twice the length $^{r}\mathbf{D}_{s}\mathbf{Y}$.

The ratios of $b:a$ for the pyrolusite parts of the intergrowths are shown in Fig. 16. At low H-insertion levels with Faradiser M, dimensions a and b are virtually identical demonstrating that initially the pyrolusite part retained an essentially tetragonal structure. The structure then hinged and $b:a$ changed to a constant value of about 1.025 for the remainder of the homogeneous H-insertion region. This hinging was probably associated with the location of H, discussed earlier, which occurred in the middle of the homogeneous H-insertion region (see Fig. 10). The fact that the hinging shown in Fig. 16 as occurring between $s=0.2$ and $s=0.25$ is at lower H-insertion level than H location, which occurred at $s=0.36$, is thought to be a further consequence of the non-equilibrium conditions pertaining during the process of insertion whereby regions adjacent to the H-insertion donor were inserted to levels higher than the overall level finally attained. For Faradiser M, the most H-inserted product was hinged even more and had a $b:a$ ratio of 1.12 and, as shown in Fig. 16, approached the ratio found in manganite.

In the companion paper,[12] lattice dimensions were not deduced for the pyrolusite part of the intergrowth when the manganese dioxide coded SBPA was H-inserted. This has now been done and the $b:a$ ratio is presented in Fig. 16. For all of the homogeneous region of H-insertion, which extends to $s=0.34$, $b<a$. The reason is that hinging took place in the direction depicted in Fig. 12 so that lattice dimension a was enhanced enabling it to match a ramsdellite a dimension, which was reduced by hinging in the opposite direction. An interesting feature of SBPA, not previously appreciated, is that in the heterogeneous region of H-insertion the pyrolusite/manganite part of the intergrowth changed from a reactant structure hinged so that $b<a$ to a product structure which was hinged in the opposite direction so that $b>a$. The coincidence of both a and c parameters for product and reactant was previously cited as reasons why H-insertion in the heterogeneous region proceeded in the b direction by movement of an almost seamless boundary. The change in hinging direction of the pyrolusite/manganite part between reactant and product may however be a reason why H-insertion in the heterogeneous region was slow for SBPA despite common a and b dimensions for reactant and product.

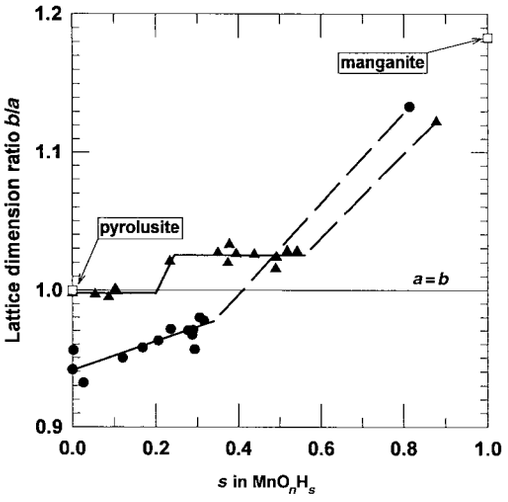

Fig. 16 Effect of H-insertion on the lattice ratio $b:a$ of the pyrolusite part of the intergrowth. ▲ Faradiser M, ● SBPA, —— homogeneous insertion, — — — heterogeneous insertion.

Conclusions

(1) H-Insertion into Faradiser M occurred homogeneously in one phase up to an insertion level of approximately $s=0.56$ and then heterogeneously in two phases up to $s=0.88$. XRD and FTIR provided independent evidence in support of this conclusion.

(2) The onset of heterogeneity for both Faradiser M and SBPA[12] coincided with expansion in the homogeneous region of the a dimension of the ramsdellite/groutite part of the intergrowth to a value which equalled the a dimension of the fully inserted product. This suggests that reagent-to-product transformation in the heterogeneous region took place in the b direction.

(3) FTIR studies showed that, like SBPA[12] and EMD,[15] no OH bonds were present at the lower levels of H-insertion with Faradiser M. However, unlike SBPA[12] and EMD,[15] H location occurred in approximately the middle of the homogeneous region at $s=0.36$. This is probably a consequence of the higher proportion of pyrolusite in the intergrowth structure of Faradiser M.

(4) Comparison of OH bending vibrations in fully H-inserted Faradiser M with spectra for groutite, manganite and fully inserted SBPA[12] clearly demonstrated the presence of a groutite/manganite intergrowth with a lower proportion of groutite than was present in fully H-inserted SBPA.

(5) H-Insertion occurred simultaneously and uniformly in both the pyrolusite and ramsdellite parts of the intergrowth and not preferentially into the ramsdellite portion. Three separate pieces of evidence support this conclusion:

- similar proportions of manganite and groutite OH bending peaks from the point of H location at $s=0.36$ until full insertion for Faradiser M,
- the coincidence of the apical expansion of ramsdellite octahedra in the homogeneous region of H-insertion for Faradiser M and SBPA, which have different proportions of ramsdellite in their intergrowths,
- the expansion of the a dimension of the ramsdellite portion of the SBPA intergrowth beyond the maximum possible hinged a dimension of uninserted pyrolusite.

(6) From conclusion (5) and an assumption of a common a dimension for the lattices of the ramsdellite/groutite and pyrolusite/manganite parts of γ-intergrowth structures, the b lattice parameter of the latter part of the intergrowth can be calculated from XRD data interpreted in terms of the former part.

(7) In the heterogeneous region of H-insertion for SBPA, the hinging of pyrolusite/manganite portions changes from a reactant in which $a>b$ to a product with $a<b$. This may be one factor why H-insertion is so much slower with SBPA than with Faradiser M.

Acknowledgement

The authors thank Professor Dom Swinkels for kindly providing the FTIR data.

References

1 O. Glemser, *Ber. Dtsch. Chem. Ges.*, 1939, **25**, 1879.
2 A. Kozawa, *Batteries Vol. 1 Manganese Dioxide*, ed. K. V. Kordesch, Marcel Dekker, New York, 1974, p. 433.
3 J. Y. Welsh and P. C. Picquet, *Progress in Batteries and Solar Cells*, Vol. 2, ed. A. Kozawa, JEC Press Inc., 1979, p. 119.
4 A. M. Byström, *Acta Chem. Scand.*, 1949, **3**, 163.
5 P. M. de Wolff, *Acta Crystallogr.*, 1959, **12**, 341.
6 D. G. Malpas and F. L. Tye, *Handbook of Manganese Dioxides Battery Grade*, ed. D. Glover, B. Schumm and A. Kozawa, IBA Inc., 1989, p. 176.
7 J. Pannetier, Y. Chabre and C. Poinsignon, *ISSI Lett.*, 1990, **1**, 5.

8 M. Ripert, J. Pannetier, Y. Chabre and C. Poinsignon, *Mater. Res. Soc. Symp. Proc.*, 1991, **210**, 359.
9 J. Pannetier, *Progress in Batteries and Battery Materials*, Vol. 11, ed. D. A. J. Swinkels and J. C. Nardi, ITE-JEC Press Inc., 1992, p. 51.
10 Y. Chabre and J. Pannetier, *Prog. Solid State Chem.*, 1995, **23**, 1.
11 E. Preisler, *J. Appl. Electrochem.*, 1989, **19**, 540.
12 L. A. H. MacLean and F. L. Tye, *J. Mater. Chem.*, 1997, **7**, 1029.
13 W. C. Maskell, J. E. A. Shaw and F. L. Tye, *Electrochim. Acta*, 1981, **26**, 1403.
14 C. St Claire-Smith, J. A. Lee and F. L. Tye, *Manganese Dioxide Symposium Vol. 1 Cleveland*, ed. A. Kozawa and R. J. Brodd, I. C. Sample Office, 1975, p. 132.
15 J. Fitzpatrick, L. A. H. MacLean, D. A. J. Swinkels and F. L. Tye, *J. Appl. Electrochem.*, 1997, **27**, 243.
16 T. Valand, *Electrochim. Acta*, 1974, **19**, 639.
17 S. Atlung, *Manganese Dioxide Symposium Vol. 1 Cleveland*, ed. A. Kozawa and R. J. Brodd, I. C. Sample Office, 1975, p. 47.
18 J. Fitzpatrick and F. L. Tye, *J. Appl. Electrochem.*, 1991, **21**, 130.
19 J. Brenet, J. Mallessan and A. Grund, *C. R. Hebd. Seances Acad. Sci.*, 1956, **242**, 111.
20 W. Feitknecht, H. R. Oswald and U. Feitknecht-Steinmann, *Helv. Chim. Acta*, 1960, **43**, 1947.
21 H. Bode, A. Schmier and D. Berndt, *Z. Elektrochem.*, 1962, **66**, 586.
22 J. P. Gabano, B. Morignat, E. Fialdes, B. Emery and J. F. Laurent, *Z. Phys. Chem. (Leipzig)*, 1965, **46**, 359.
23 T. Kohler, T. Armbruster and E. Libowitzky, *J. Solid State Chem.*, 1997, **133**, 486.
24 R. M. Potter and G. R. Rossman, *Am. Mineral.*, 1979, **64**, 1199.
25 W. C. Maskell, J. E. A. Shaw and F. L. Tye, *J. Power Sources*, 1982, **8**, 113.
26 W. C. Maskell, J. E. A. Shaw and F. L. Tye, *Electrochim. Acta*, 1983, **28**, 225.
27 F. L. Tye, *Electrochim. Acta*, 1985, **30**, 17.
28 F. L. Tye, *Electrochim. Acta*, 1976, **21**, 415.
29 J. H. A. Laudy and P. M. de Wolff, *Appl. Sci. Res.*, 1963, **B10**, 157.
30 G. Vaux and H. Bennett, *Mineral. Mag.*, 1937, **24**, 521.
31 H. Strunz, *Naturwissenschaften*, 1943, **78**, 89.
32 L. A. H. MacLean, PhD thesis, Middlesex University, 1993.
33 JCPDS card 39-375.
34 JCPDS card 24-713.